Stratospheric Aerosol Measurements III: Optical Model Calculations

R. G. PINNICK, J. M. ROSEN AND D. J. HOFMANN

Department of Physics and Astronomy, University of Wyoming, Laramie 82071

(Manuscript received 9 June 1975, in revised form 20 October 1975)

ABSTRACT

Mie single scattering, absorption, and total extinction calculations for various size distribution and composition models of the stratospheric aerosol are presented. These models are derived from global *in-situ* measurements made with a balloon-borne photoelectric particle counter during the period December 1971 through July 1974. The models are in agreement with simultaneous aerosol mass measurements made by aircraft filter sampling and by balloon-borne impactor over Laramie, Wyo. Nominal stratospheric aerosol optical depths at 0.53 μm wavelength are 0.005 to 0.007. The maximum stratospheric aerosol absorption cross section at this wavelength is 0.04×10^{-3} km^{-1} at 18–20 km altitude, assuming a refractive index imaginary part of 0.01. The predicted 180° backscatter lidar return at the 18–20 km altitude of maximum aerosol mixing ratio is 9% to 17% of the Rayleigh return at a wavelength of 0.6943 μm for the various aerosol models. Measured and predicted lidar returns over Laramie in September 1972 are in good agreement for several of the size distribution and composition models used here. Values of the global stratospheric aerosol albedo at 0.53 μm are 0.002 to 0.003.

1. Introduction

Articles in the literature dealing with light scattering properties of atmospheric aerosols are numerous and of great variety. Many fall into two general categories: those in which the effect of aerosols on radiative transfer processes in the atmosphere is studied (Plass and Kattawar, 1972; Shettle and Green, 1974; Braslau and Dave, 1973a, b; Sargent and Beckman, 1973; Liou, 1973; Yamamoto and Tanaka, 1972; Rasool and Schneider, 1971) and those in which aerosol size distribution or composition information is obtained (or shown possible to be obtained) from light scattering measurements in the atmosphere (Elterman *et al.*, 1973; Harrison *et al.*, 1972; Tashenov *et al.*, 1973; Zuyev *et al.*, 1973; Green *et al.*, 1972; Ward *et al.*, 1973; Prishivalko and Naumenko, 1973; Latimer, 1972; Grams *et al.*, 1972, 1974; Pilipowskyj *et al.*, 1968; Bhardwaja *et al.*, 1974; de Bary and Rossler, 1966). The results reported here, although limited to the stratospheric aerosol layer, are believed to be based on the most consistent and globally extensive measurements of the aerosol size distribution made to date. From this comprehensive set of data and other data on aerosol composition, we have constructed appropriate optical models which are used in Mie single scattering calculations of the aerosol total extinction, absorption, 180° lidar backscattering, angular scattering, outward (2π hemispheric) scattering for a given solar zenith angle, and global stratospheric aerosol albedo.

2. Size distribution and composition models

The size distribution models are derived from extensive global measurements of the stratospheric aerosol described in some detail in earlier papers (Hofmann *et al.*, 1975; Rosen *et al.*, 1975) utilizing a balloon-borne forward scattering photoelectric particle counter originally used for stratospheric measurements by one of the authors (Rosen, 1964). The counter has been calibrated in the laboratory with various monodisperse aerosols of known size and refractive index (Pinnick *et al.*, 1973). Slightly nonspherical particles do not grossly affect the counter calibration for particles with diameter $\lesssim$0.5 μm. The counter efficiency has also been investigated (Pinnick and Hofmann, 1973). In the normal balloon flight configuration with this instrument, only two particle size ranges are measured: diameters greater than 0.3 μm and 0.5 μm. On occasion, during soundings at Laramie, particles having diameters $>$0.25 μm, 0.28 μm, 3 μm and 5 μm were also measured. For particle refractive indexes with real part between 1.40 and 1.60 and with absorptive (imaginary) part less than 0.05, the size calibration for particles with diameter $\lesssim$0.5 μm is not sensitive to the refractive index. For an extensive discussion of the detector and the credibility of the calibration, see Hofmann *et al.* (1975).

Table 1 lists the location and number of aerosol soundings used in this analysis. Data from these soundings for the particles counted with diameter greater than 0.3 μm and 0.5 μm, presented as a concentration ratio, are shown in Figs. 1 (for Laramie) and 2 (for all other stations). The measurements were taken over a period of about two years from December 1971 through February 1974, and were discussed in detail by Rosen *et al.* (1975) and Hofmann *et al.* (1975). The bars mark the range of the measured tropopause altitudes. Al-

TABLE 1. Location and number of aerosol soundings.

Station	Latitude	Number of soundings
Ice Island T-3	~85°N	3
Barrow, Alaska	71.3°N	4
Ft. McMurray, Alberta	57.4°N	5
Duluth, Minnesota	46.7°N	2
Laramie, Wyoming	41.2°N	22
Palestine, Texas	31.8°N	5
Albrook AFB, Panama	9°N	4
Longreach, Australia	23.5°S	2
Mildura, Australia	34.2°S	2
McMurdo Station, Antarctica	77.2°S	2
South Pole Station, Antarctica	90°S	3

though this ratio fluctuates from less than 2 to more than 40 in the troposphere for many of the soundings shown, in the stratospheric aerosol layer it is remarkably constant and nearly independent of latitude. This implies a relatively uniform and quasi-constant size distribution, at least in the size range 0.3 to 0.5 μm diameter.

There appears to be a small but definite decrease in the ratio with altitude between 12 and 23 km, decreasing from an average value of about 5 to 4. This corresponds to a variation in the e-folding radius (radius

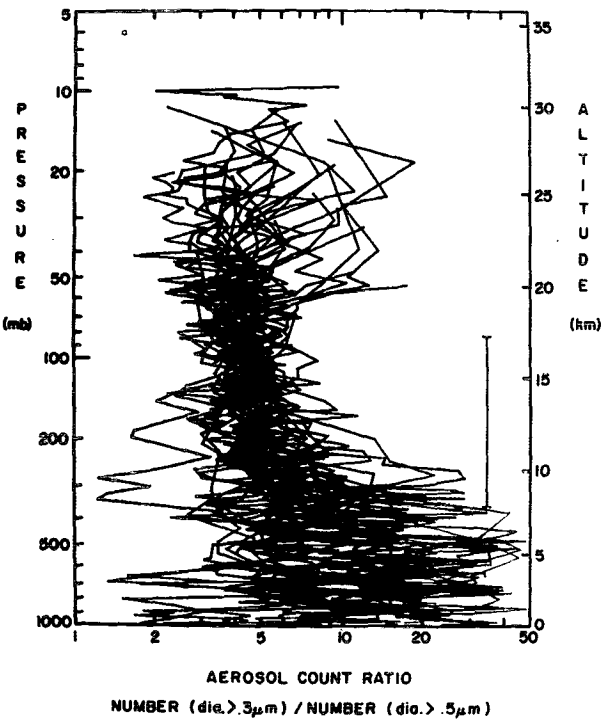

FIG. 2. As in Fig. 1 except for 32 balloon flights at stations listed in Table 1 (except Laramie).

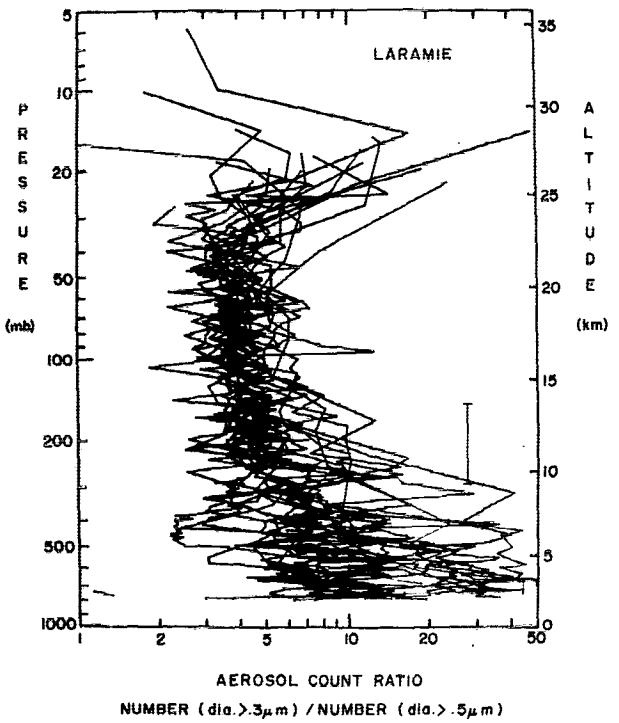

FIG. 1. Aerosol concentration ratio determined by photoelectric particle counter [number (dia>0.3 μm)/number (dia>0.5 μm)] versus pressure for 22 balloon flights over Laramie from December 1971 through February 1974. The vertical bar marks the range of the observed tropopause heights.

interval over which the concentration changes by a factor of e) from 0.07 to 0.08 μm. The cause of this apparent variation in the size distribution is unknown. Sedimentation effects would suggest the opposite. A variation with altitude in the aerosol particle production processes, e.g., chemical reaction, condensation and coagulation, could presumably affect the size distribution; however, little is known concerning these phenomena in the stratosphere.

The Laramie data suggest a rather abrupt change in the size distribution between about 23 and 25 km, with a relative increase of small particles. This change is not apparent in the data from the other stations. The large fluctuations in the ratio above 25 km are not significant since smaller numbers of particles are encountered in this region necessitating longer integration intervals and consequently a less than adequate comparison of the two sizes in forming the ratio.

From these data a global-average value for the 0.3 to 0.5 μm diameter integral particle concentration ratio, at 18–20 km, is 4.0$\pm$0.5. Similar data for the relative integral concentration of 0.25 and 0.28 μm diameter particles measured in five soundings at Laramie from December 1971 through February 1974 also show a relatively constant particle size distribution in this size range.

The data are summarized in Fig. 3 in which the integral size distribution for the nominal peak con-

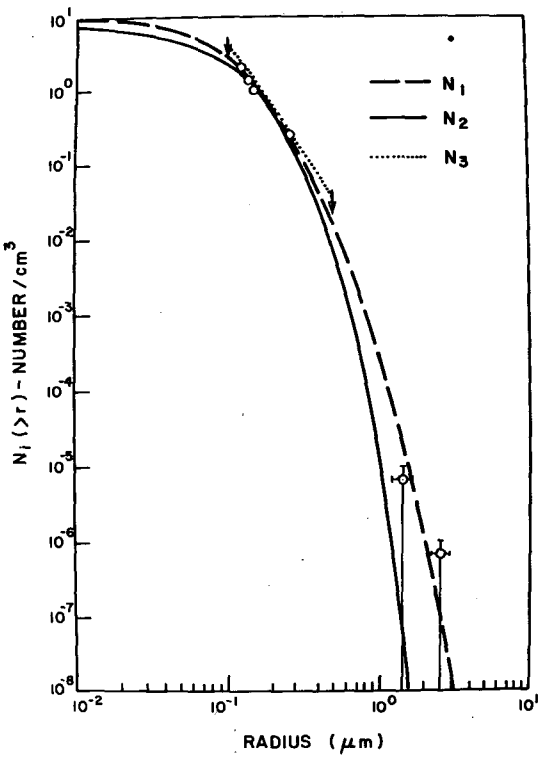

FIG. 3. Integral particle concentration versus particle radius measured by photoelectric particle counter for the 1971–74 period. The data are approximated by log-normal (N_1), exponential (N_2), and restricted power law (N_3) size distribution functions.

centration of stratospheric aerosol at 18–20 km for the period 1971–73 is shown. The errors in determination of particle size and relative particle concentrations, with exception of the measurement of the 3 and 5 μm diameter particles, are about half the diameter of the circles making the measurements. The concentration of 3 and 5 μm diameter particles was measured during a single sounding over Laramie, in July 1974, with a photoelectric particle counter similar to the one used for measurement of the smaller particles, but with a much higher sampling rate ($\sim$1 liter per second). The loss of particles in the intake tube due to impaction and settling was estimated to be relatively small at 20 km. As indicated in Fig. 3, concentration measurements of these larger particles are only upper limits.

The smooth curves shown in Fig. 3 are log-normal, exponential, and restricted power law integral size distribution function fits to the data. These size distribution functions were used in the optical calculations to be presented in the next section. Their specific forms are:

$$N_1(>r)=\frac{N_0}{(2\pi)^{\frac{1}{2}}\ln\sigma_g}\int_r^\infty \exp\left[-\left(\frac{\ln r'/r_g}{2^{\frac{1}{2}}\ln\sigma_g}\right)^2\right]\frac{1}{r'}dr',$$

where $N_0=10$ cm^{-3}, $\sigma_g=1.86$, $r_g=0.0725$ μm;

$$N_2(>r)=N_0e^{-r_0},$$

where $N_0=8.44$ cm^{-3}, $r_0=0.075$ μm; and

$$N_3(>r)=N_0\left(\frac{r}{r_0}\right)^{-\alpha},\quad 0.1\ \mu\text{m}\leqslant r\leqslant 0.5\ \mu\text{m},$$

where $N_0=4.34$ cm^{-3}, $r_0=0.1$ μm, $\alpha=3$. $N_i(>r)$ is the particle concentration for particles with radius $\geqslant r$. The power law distribution has been cut off at $r=0.1$ and 0.5 μm. The values of the parameter N_0 have been adjusted so that for each size distribution there is 1 particle cm^{-3} with diameter >0.3 μm, the condition for the nominal peak aerosol concentration at 18–20 km altitude for the 1971–73 period. These particle size distributions represent the range of size distribution information that can be extracted from the optical counter data. For the smaller and larger size ranges the size distribution models differ significantly. Calculated values of the total stratospheric aerosol concentration of all sizes obtained from these size distributions are 10, 8.44 and 4.34 particles cm^{-3}, respectively. These values are consistent with recent measurement of stratospheric condensation nuclei ($r>0.01$ μm) made by Rosen and Hoffmann (1974). Thus the model size distributions N_1 and N_2 are apparently consistent with measurements from about 0.02 to 5 μm diameter.

In order to calculate mass concentrations and scattering data from these size distributions, knowledge of the composition and index of refraction of the aerosol is necessary. An approximate refractive index has been determined for the stratospheric aerosol from some of the photoelectric particle counter measurements by judiciously setting a discriminator level in the region of double-valued response. To indicate the method of refractive index determination the reader is directed to Fig. 4 in which the counter response for a number of different particle refractive indexes is shown. The positions of the discriminator level settings used are marked by arrows and labeled channel 1, 2 and 3 for convenience. For a given aerosol size distribution, the relative number of particles counted with response greater than the channel 3 discriminator level setting is sensitive to the particle refractive index. For example, for aerosol with refractive index $1.40-0i$, particles with diameters between 0.76 and 1.0 μm as well as particles with diameter >1.5 μm are counted in channel 3. In contrast, for aerosol with refractive index $1.50-0i$, only particles with diameter >1.4 μm are counted in channel 3. For a particle size distribution that falls off in the 0.3 to 2 μm diameter size range, the net result is that the number of particles counted in channel 3 relative to the number in channel 2 is a measure of the aerosol refractive index, at least in the range $1.40-0i$ to $1.50-0i$. In order to make this measurement quantitative, polydisperse spherical aerosols with various known refractive indexes and size distributions have been measured in the laboratory using a photoelectric particle counter with discriminator

levels set as in Fig. 4. The results, summarized in Fig. 5, show the ratio of particles counted in channel 2 to those in channel 3, as a function of the ratio of particles counted in channel 1 to those in channel 2. This latter ratio is a measure of the aerosol size distribution that is nearly independent of refractive index, as can be seen from the counter response curves. If the data for the various indexes of refraction are approximated by straight lines, then the slopes of these lines approximately characterize the aerosol refractive index, independent of size distribution. These slopes are only slightly different for refractive indexes from $1.33-0i$ to $1.42-0i$. However, since the slope changes rapidly in the range $1.46-0i$ to $1.53-0i$, the refractive index measurement by this technique is more definitive in this range.

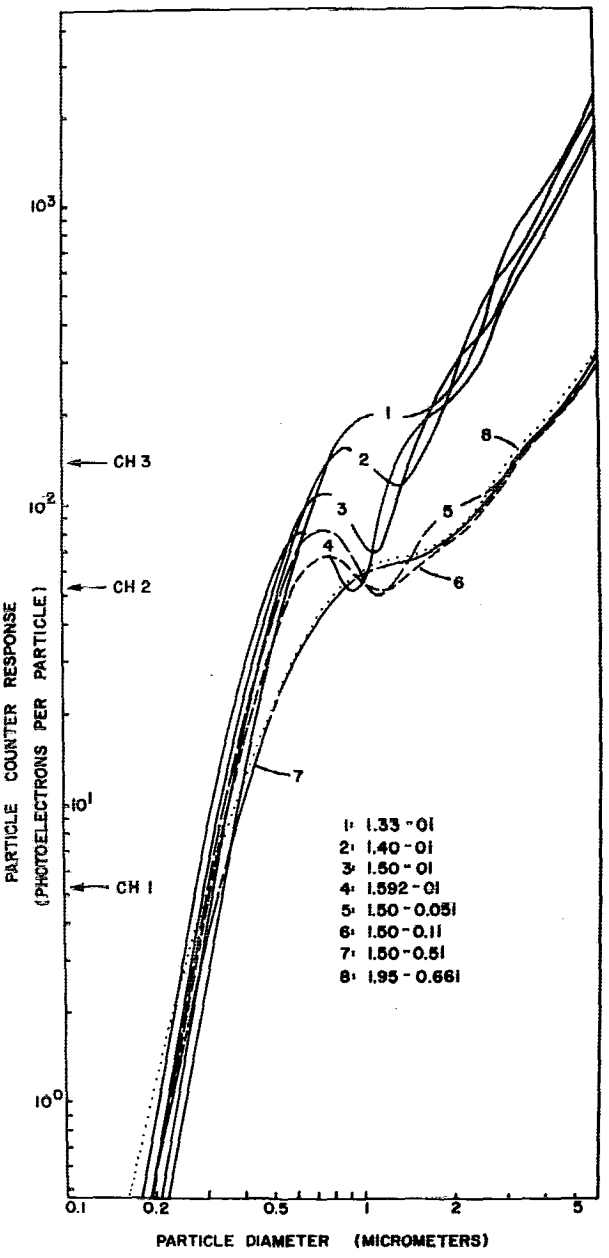

FIG. 4. Photoelectric particle counter response versus particle diameter for several aerosol refractive indexes. The particle size discriminator levels are set as marked at 5.3 photoelectrons per particle (channel 1), 53 photoelectrons per particle (channel 2), and 140 photoelectrons per particle (channel 3).

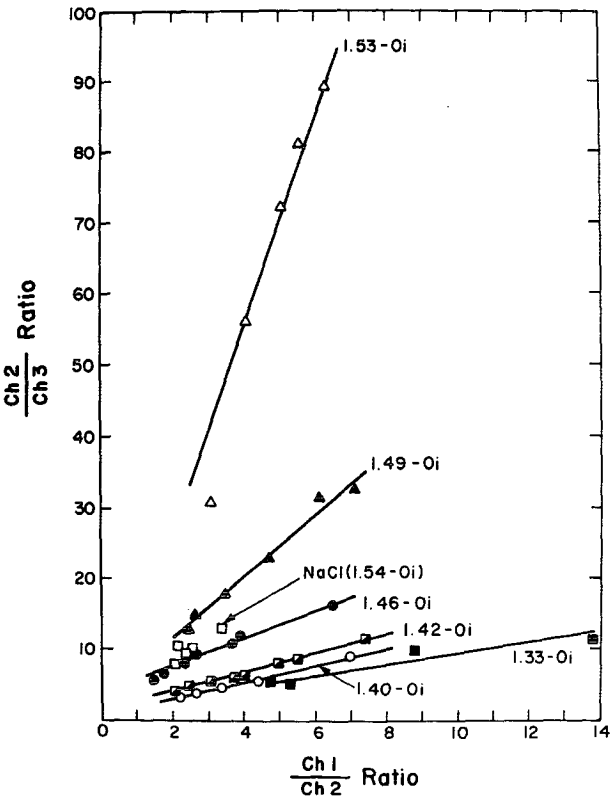

FIG. 5. Photoelectric particle counter measurements of aerosol concentration ratios: (channel 1/channel 2) versus (channel 2/channel 3) for laboratory generated aerosols with various refractive indexes. All measurements are on spherical particles except for the NaCl measurements designated by the open squares. The slopes of the lines approximating the data are used for the refractive index determination.

The aerosol refractive index as determined by this technique for three balloon flights over Laramie in spring and summer of 1974, and one flight over Holoman AFB, Texas, in May 1974, are summarized in Fig. 6. The parameter plotted versus pressure in this figure is the ratio of the square of the channel 2 particle concentration to the product of the channel 1 and channel 3 concentrations, which is approximately the slope discussed earlier and is a measure of the aerosol refractive index, independent of particle size distribution. The corresponding refractive indexes, as determined from Fig. 5, are marked on the abscissa. The vertical bar marks the range of tropopause heights. The analysis assumed spherical aerosol (since the method is based on measurement of spherical aerosols generated in the laboratory), and furthermore requires

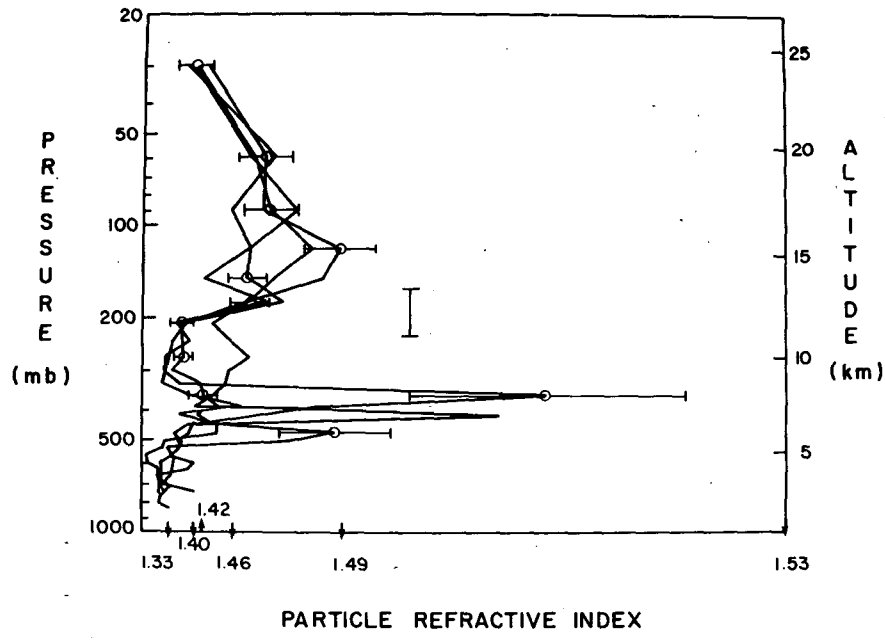

FIG. 6. Pressure versus aerosol refractive index determined by photoelectric particle counter for three balloon flights over Laramie during spring and summer of 1974 and one over Holoman AFB, Alamagordo, N. Mex., May 1974. The verticle bar marks the range of observed tropopause heights. The parameter plotted on the abscissa is the particle concentration ratio: (channel 2)^2/(channel 1·channel 3). The indexes plotted on the abscissa are determined from Fig. 5. See text for explanation.

that the channel 1 to channel 2 ratio, as measured in the laboratory, uniquely characterizes the size distribution of the atmospheric aerosol sampled in flight. Since the channel 3 discriminator level is set for particles large enough for shape to be important, the refractive index determination is probably meaningless for nonspherical aerosol. The failure of the refractive index determination technique for nonspherical particles is demonstrated in Fig. 5 in which data for NaCl aerosol ($1.54-0i$) nearly match those of spherical particles with index $1.46-0i$. The NaCl aerosol are primarily cubic in shape. The indication from these limited results is that the refractive index determined by this technique is low for nonspheres, possibly explaining the generally low values measured in the troposphere in Fig. 6. For absorptive aerosol with refractive index imaginary part less than 0.01, the technique should be relatively insensitive to particle absorption.

The typical error bars shown in Fig. 6 are for one standard deviation counting statistics only and do not reveal uncertainties discussed in the preceding paragraph. Under the assumption of spherical particles the aerosol refractive index is close to that of water in the troposphere, except for relatively thin layers of aerosol with higher refractive index. In the stratosphere, the measurements indicate a refractive index in the 1.40 to 1.49 range, being about 1.46 at 18–20 km and decreasing to around 1.40 at 20 km. Again it should be emphasized that the refractive index determination is probably meaningless for nonspherical particles. Furthermore, the technique assumes all the aerosol at a given altitude is characterized by a unique refractive index.

These measurements of the stratospheric aerosol refractive index are in agreement with more direct measurements of the aerosol composition made with a balloon-borne particle impactor provided by K. Bigg [see Bigg *et al.* (1970) for details of the impactor]. Measurements of the composition were made with this instrument simultaneously with the photoelectric counter on a number of occasions at Laramie. Specially prepared electron microscope grids rotated through the air sample stream during balloon ascent allowed for both composition and vertical profile measurements. Size distribution and vertical profile data thus obtained by Bigg were in agreement with those obtained by the photoelectric counter. Analysis of the reactions on the grids indicated the presence of ammonium sulfate, ammonium persulfate and sulfuric acid in the stratospheric layer with a preponderance of free acid in the higher stratosphere (Bigg, 1975).

Previously Rosen (1971) measured the boiling point of the stratospheric aerosol and found values in agreement with a 75% sulfuric acid, 25% water composition. In view of the somewhat direct measurements of aerosol composition by Bigg, the refractive index measurements with the particle counter in this work, and the measurement of aerosol boiling point by Rosen, the stratospheric aerosol refractive index for visible

light can be best characterized as having a real part in the range 1.40 to 1.50, an absorptive part of 0.05 or less, and a density of about 1.5 g cm^{-3}.

The equivalent mass concentrations for the size distributions in Fig. 3, assuming an aerosol density of 1.5 g cm^{-3}, are 0.14×10^{-12}, 0.13×10^{-12} and 0.13×10^{-12} g cm^{-3}. These values are in good agreement with measurements obtained by aircraft filter samples collected at 18.2 km over Laramie on 13–14 September 1972 by the Los Alamos Aerosol Research Group. Chemical analysis of the filter samples for SO_4, calcium, sodium, chlorine and magnesium revealed a total mass concentration of 0.13×10^{-12} g cm^{-3} (W. Sedlacek, private communication). Results of scanning electron microscopy indicate that more than 99% of the particle mass was absorbed into the filter fibers as liquid.

3. Scattering calculation details and results

Mie single scattering calculations for the stratospheric aerosol models described in the previous section are outlined and the results presented here. The total extinction, total absorption, 180° backscatter, and angular scattering cross sections are as follows:

$$\beta_e^{(i)}=\int_0^\infty \pi r^2 Q_e n_i(r)dr$$

$$\beta_a^{(i)}=\int_0^\infty \pi r^2 Q_a n_i(r)dr$$

$$\beta_{180}^{(i)}=\frac{1}{2k^2}\int_0^\infty [i_1(x, m, \theta=180°) + i_2(x, m, \theta=180°)]n_i(r)dr$$

$$\beta_1^{(i)}(\theta)=\frac{1}{k^2}\int_0^\infty i_1(x,m,\theta)n_i(r)dr$$

$$\beta_2^{(i)}(\theta)=\frac{1}{k^2}\int_0^\infty i_2(x,m,\theta)n_i(r)dr.$$

Here

$$n_i(r)=\frac{d}{dr}N_i(>r), \quad x=\frac{2\pi r}{\lambda},$$

where $N_i(>r)$ are the integral particle size distributions introduced earlier, Q_e and Q_a are the Mie efficiency factors defined as the ratios of single particle extinction and absorption cross sections to the particle geometric cross section, and i_1 and i_2 are the Mie intensities associated with the intensities of light scattered with electric vector perpendicular and parallel, respectively, to the plane of scattering. They are functions of the particle size parameter x, the complex particle refractive index m, and the angle of scattering θ from the forward direction. The parameter k is the wavenumber of the incident light. The angular scattering cross sections

TABLE 2. Predicted value of the total extinction cross sections $(10^3 \text{ km})^{-1}$ at 0.53 μm wavelength for the nominal peak stratospheric aerosol concentration at 18–20 km altitude during the 1971–73 period. The bracket marks the range of realistic values of the refractive index.

Aerosol refractive index	Size distribution model N_1	N_2	N_3
1.33−0i	0.377	0.422	0.360
1.40−0i	0.491	0.537	0.477
1.43−0i	0.539	0.581	0.524
1.50−0i	0.641	0.670	0.623
1.50−0.001i	0.641	0.670	0.623
1.50−0.002i	0.641	0.670	0.623
1.50−0.005i	0.641	0.668	0.622
1.50−0.01i	0.641	0.666	0.622
1.50−0.02i	0.641	0.662	0.621
1.50−0.05i	0.643	0.652	0.620
1.50−0.1i	0.649	0.641	0.624
1.50−0.5i	0.765	0.674	0.713
1.60−0i	0.764	0.763	0.737

$\beta_1^{(i)}(\theta)$ and $\beta_2^{(i)}(\theta)$ are for incident polarized light with electric vector perpendicular and parallel to the scattering plane. These will be referred to as the cross sections for perpendicular and parallel polarization. The corresponding cross section for natural light is $[\beta_1^{(i)}(\theta)+\beta_2^{(i)}(\theta)]/2$. The Mie parameters in the above cross sections were calculated with a program written by Dave (1968) using the mesh on size parameter x: 0.1 to 1.0 in steps of 0.01, 1.02 to 3.0 in steps of 0.02, 3.1 to 10 in steps of 0.1, and 10.2 to 50 in steps of 0.2. For the size distributions used here, more than 99% of the particles in the above integrations are for a mesh in size parameter x of 0.1 or finer and therefore meet the criterion of tolerable reliability described by Dave (1969a, b).

Values of the total extinction cross sections at 0.53 μm wavelength for the nominal peak stratospheric aerosol concentration at 18–20 km altitude are found in Table 2 for the size distributions studied. The extinction cross sections for various model size distributions for a single refractive index differ by, at most, about 10%. Therefore, the optically important region of aerosol particle size, at least for extinction, is from 0.3 to 1 μm diameter, since in this region of particle size the various model size distributions are in approximate agreement. The cross sections are slightly sensitive to the particle refractive index real part, but insensitive to the imaginary parts within a realistic range of values of the imaginary part. The wavelength dependence of these cross sections is approximately λ^{-1} in the visible region, as can be seen from Fig. 7. In this figure the extinction cross section wavelength dependence is shown for several size distribution-refractive index combinations. An approximate mean stratospheric optical depth can be obtained by multiplying these cross sections by 10^6 cm, the condition for 10^6 particles with diameter ≥ 0.3 μm per centimeter squared-column above the tropopause, the average

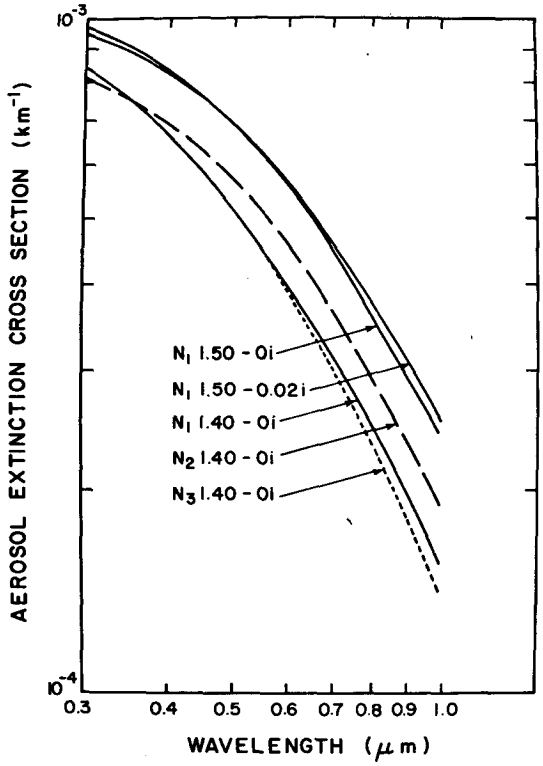

FIG. 7. Predicted values of the stratospheric aerosol extinction cross section versus wavelength for several size distribution and composition models of the stratospheric aerosol. The cross sections in this figure and in Figs. 8 and 11–13 are for the nominal peak aerosol concentration at 18–20 km altitude for the 1971–73 period.

aerosol loading observed over Laramie during 1971–73 (Hofmann *et al.*, 1975). The maximum optical depth for the stratospheric aerosol using the models described here is 0.01. For optical depths in this range, Deepak and Green (1970) have shown that double scattering is unimportant compared to single scattering. Therefore, single scattering calculations are considered sufficient for the stratospheric aerosol optical modeling done here.

Values of the absorption cross sections at 0.53 μm wavelength, again for the nominal peak stratospheric aerosol concentration at 18–20 km altitude, are found in Table 3. These cross sections are nearly proportional to the refractive index absorptive part, but very nearly independent of size distribution. As stated previously, refractive index absorptive parts >0.05 are probably not realistic for stratospheric aerosol.

TABLE 3. As in Table 2 except for the absorption cross sections $(10^3 \text{ km})^{-1}$.

Aerosol refractive index	Size distribution model N_1	N_2	N_3
1.50−0*i*	0	0	0
1.50−0.001*i*	0.00382	0.00388	0.00346
1.50−0.002*i*	0.00758	0.00769	0.00687
1.50−0.005*i*	0.0185	0.0188	0.0169
1.50−0.01*i*	0.0358	0.0363	0.0328
1.50−0.02*i*	0.0673	0.0677	0.0621
1.50−0.05*i*	0.143	0.142	0.134
1.50−0.1*i*	0.232	0.222	0.217
1.50−0.5*i*	0.473	0.401	0.430

TABLE 4. Predicted values of the backscatter cross section (180°) at 0.6943 μm wavelength for the nominal peak stratospheric aerosol concentration (during 1971–73) at 18–20 km altitude, shown as a percentage of the Rayleigh scattering at 18 km using the 1962 Standard Atmosphere molecular density. The bracket marks the range of realistic values of the refractive index.

Aerosol refractive index	Size distribution model N_1	N_2	N_3
1.33−0*i*	5.8	5.8	5.7
1.40−0*i*	9.1	9.4	8.9
1.43−0*i*	11.0	11.3	10.5
1.50−0*i*	17.0	17.2	14.8
1.50−0.001*i*	16.6	16.9	14.5
1.50−0.002*i*	16.3	16.5	14.5
1.50−0.005*i*	15.3	15.5	13.7
1.50−0.01*i*	14.0	14.1	12.8
1.50−0.02*i*	11.9	11.7	11.2
1.50−0.05*i*	8.2	7.5	8.3
1.50−0.1*i*	5.9	4.8	6.2
1.50−0.5*i*	6.9	5.1	7.1
1.60−0*i*	30.5	31.6	23.1

Values of the backscatter cross section (180°) at 0.6943 μm for the nominal peak stratospheric aerosol

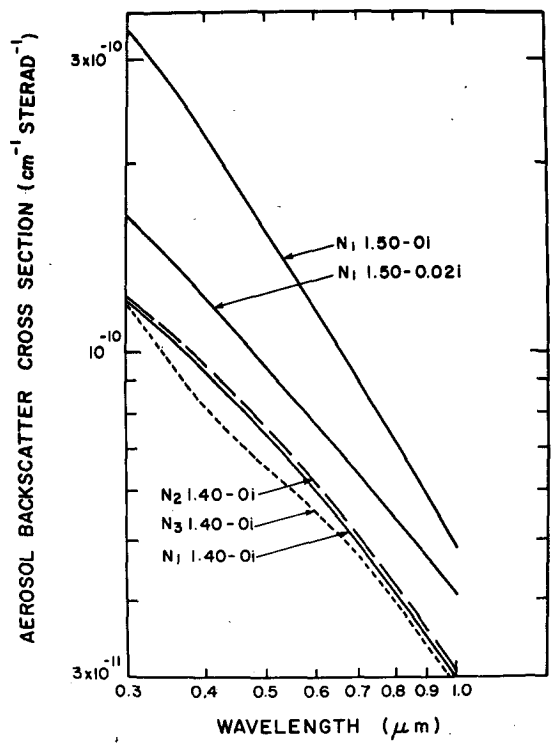

FIG. 8. As in Fig. 7 except for stratospheric aerosol backscatter cross section.

concentration at 18–20 km altitude, presented as a percentage of the Rayleigh scattering at 18 km using the 1962 Standard Atmosphere molecular density (*U. S. Standard Atmosphere Supplements, 1966*) are shown in Table 4. These values are predicted lidar returns and are relatively sensitive to the aerosol refractive index, but again rather insensitive to particle size distribution. If the stratospheric aerosol particles are not homogeneous spheres, as suggested by Bigg (1975), these predictions could be significantly in error. For realistic refractive indexes the wavelength dependence of these backscatter cross sections for $0.4\ \mu m \leqslant \lambda \leqslant 1\ \mu m$ is again approximately λ^{-1}, as is evident from Fig. 8. This relative insensitivity of the wavelength dependence of the backscatter cross sections to size distribution and refractive index means that two-color lidar measurements will not be definitive in determining aerosol particle size distribution or refractive index.

A comparison of observed and predicted lidar returns for the stratospheric aerosol over Laramie on 13–14 September and 15–16 September 1972, are presented in Figs. 9 and 10. The predicted lidar returns are based on the log-normal size distribution (N_1) for refractive index $1.40-0i$, and are scaled by the altitude-dependent aerosol concentration as measured *in situ* by balloon-borne photoelectric particle counter. The simultaneous lidar measurements were made and analyzed by NASA-LRC and details of the system and of the measurements have been presented elsewhere (Northam *et al.*, 1974). In view of the fact that the measured and predicted lidar returns are absolute, with no renormalization of data for a best fit of the profiles, the comparison is good. Also shown in Fig. 9

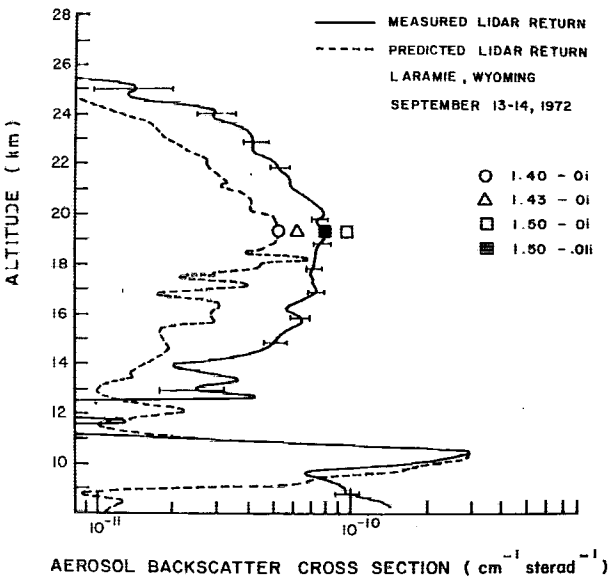

FIG. 9. Measured and predicted lidar returns over Laramie. The predicted return is for a log-normal size distribution and for refractive index $1.40-0i$. Predicted returns at 19 km for several other refractive indexes are shown.

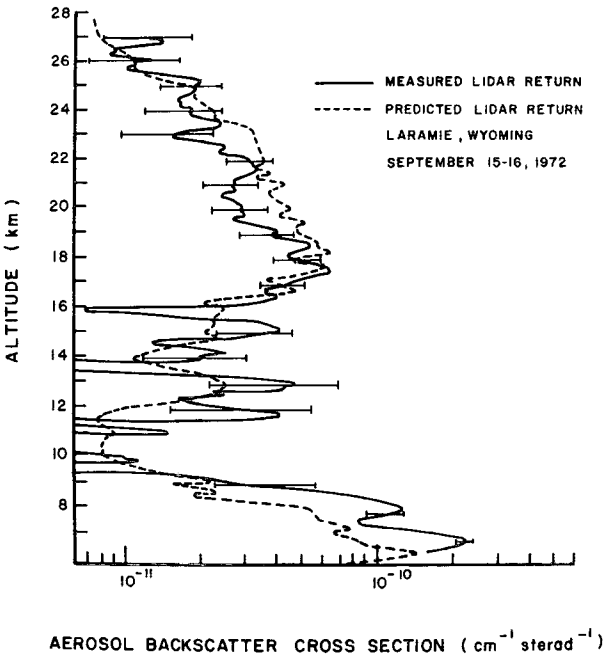

FIG. 10. As in Fig. 9 without predicted returns for other refractive indexes.

are the predicted lidar returns at 19 km for several other refractive indexes. As can be seen from Table 4, the corresponding returns for other size distribution models are not significantly different from the log normal. It should be noted that the predicted lidar returns (dashed curves) shown in both figures are for the same aerosol model size distribution (N_1) and refractive index ($1.40-0i$) yet the predicted and measured lidar returns in Fig. 10 are in much better agreement. No obvious reason for this discrepancy exists.

Angular scattering cross sections for the three size distributions for light polarized perpendicular and parallel to the scattering plane are shown in Fig. 11 for refractive index $1.43-0i$. All the angular cross sections presented here are at 0.53 μm wavelength and are for the nominal peak stratospheric aerosol concentration at 18–20 km altitude. The respective cross sections are nearly the same for all size distributions but have a different angular dependence for scattering angles $>60°$ from the forward direction. Angular scattering cross sections for the log-normal size distribution for several refractive indexes are shown in Figs. 12 and 13 for perpendicular and parallel polarizations, respectively. Corresponding results for the other size distributions are not significantly different and therefore are not shown. Increased real part of the refractive index causes more backward scattering but leaves the forward scattering approximately the same as expected from geometrical optics. Particle absorption causes less backscattering, but again does not change the forward scattering appreciably.

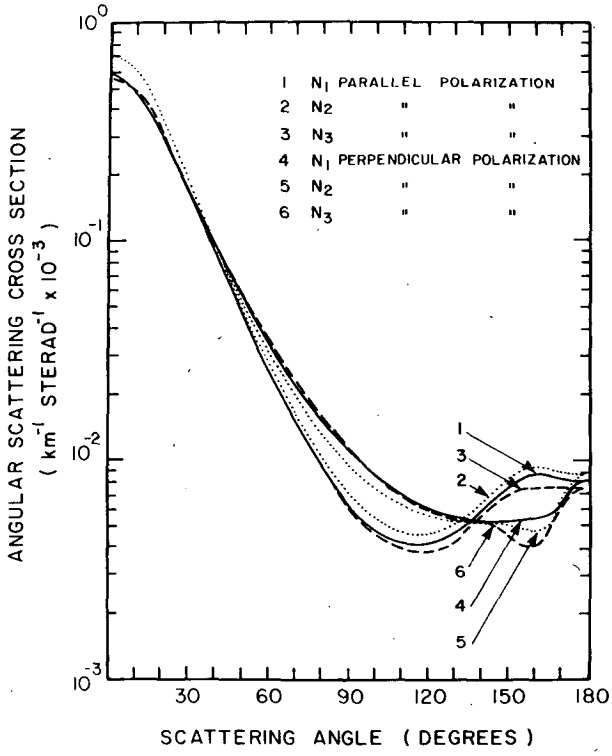

FIG. 11. Aerosol angular scattering cross sections for perpendicular and parallel polarized light versus scattering angle for refractive index $1.43-0i$. See legend to Fig. 3 for definitions of N_1, N_2 and N_3.

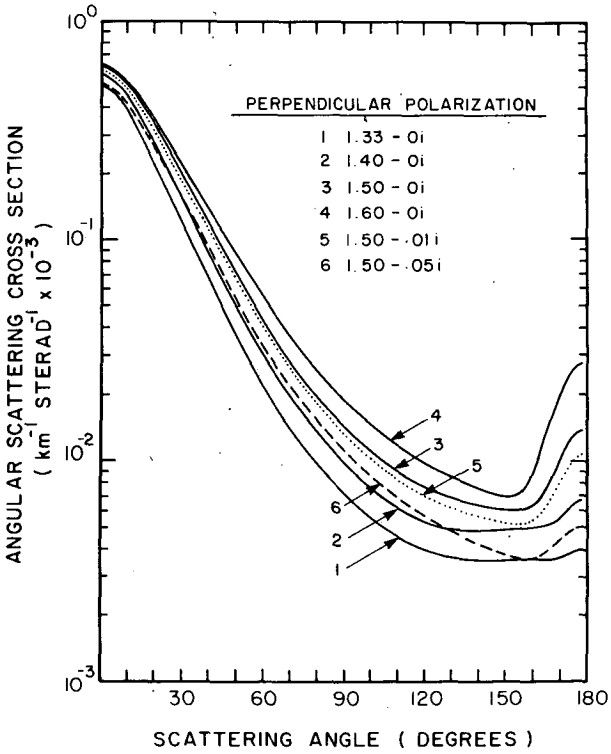

FIG. 12. Aerosol angular scattering cross sections for perpendicularly polarized light versus scattering angle for several particle refractive indexes and for a log-normal size distribution.

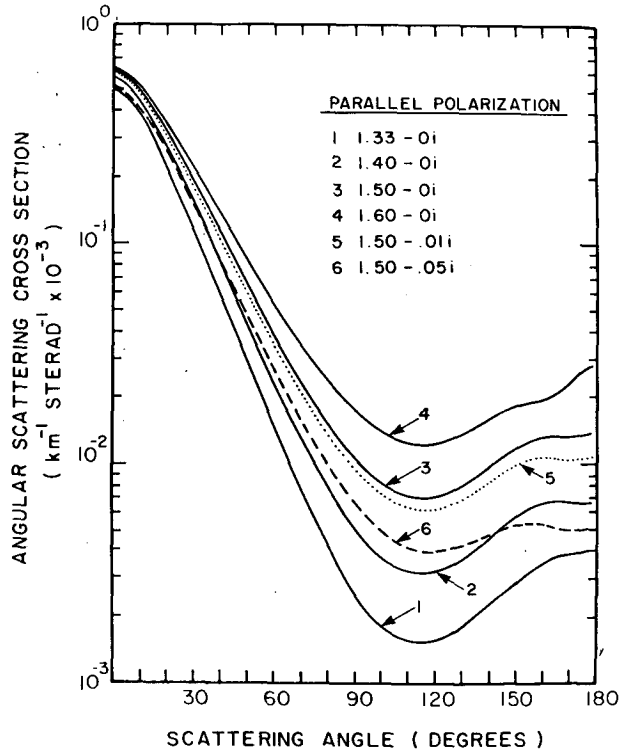

FIG. 13. As in Fig. 12 except for parallel polarized light.

The final optical scattering calculations presented here for the stratospheric aerosol are the 2π hemispheric "outscatter" cross sections for various solar zenith angles. This cross section is for the radiation scattered by the stratospheric aerosol in the 2π hemisphere away from the earth and is of interest since the scattered light in question does not enter into the radiative transfer processes in the atmosphere-earth-ocean system below the stratosphere. The outscatter cross section is

$$\beta_{2\pi}^{(i)}=\frac{1}{2k^2}\int_{\Omega}d\Omega'\int_{0}^{\infty}[i_1(x,m,\theta)+i_2(x,m,\theta)]n_i(r)dr.$$

The 2π solid angle in question is Ω, and $n_i(r)$ is again the differential particle size distribution. This cross section has been calculated by averaging over the mesh in size parameter given earlier, and for 1° angular increments. Values of this cross section as a function of solar zenith angle, shown as the fraction of solar radiation outscattered by a globally uniform layer of the stratospheric aerosol for the condition of 10^6 particles with diameter $\gtrsim 0.3$ μm per centimeter squared-column above the tropopause, are found in Fig. 14. The curves shown for the various refractive indexes are all for the log-normal size distribution (N_1). The form of the results for the other size distributions is not significantly different. The relatively large increase in solar radiation outscattered toward a 90° zenith angle is a result of the preponderance of forward scattering by the aerosol and of the greater aerosol optical

depth for larger zenith angles. For a 90° zenith angle, one-half the total radiation scattered by the stratospheric aerosol is scattered in the 2π hemisphere away from the earth. Global average values of the hemispheric outscattering, properly weighted, are given in Table 5. These values can be interpreted to be the stratospheric aerosol albedo. As is seen from the table, the albedos are generally between 0.002 and 0.003 for realistic refractive indexes. Roughly half the outscattered radiation is for zenith angles $\geqslant 70°$. For increases in the stratospheric aerosol loading by a factor 3 or less, and for constant size distribution, and of course assuming homogeneous spherical particles, these numbers can be scaled by the increase in total aerosol without large error from effects of multiple scattering.

An important point bearing on all the optical model calculations presented here is that in addition to the assumption of homogeneous spherical particles, the models further assume the aerosol is characterized by a single refractive index at a particular altitude or range of altitudes. Since the Mie theory is not linear, valid scattering or absorption cross sections for a multicomposition aerosol necessitates consideration of the individual refractive indexes of the respective components. This is in part the reason Mie results are presented for a relatively large range of refractive index values. If, in fact, the stratospheric aerosol is a multicomposition aerosol, these results serve as a guideline for the range of optical properties of the aerosol in the visible region.

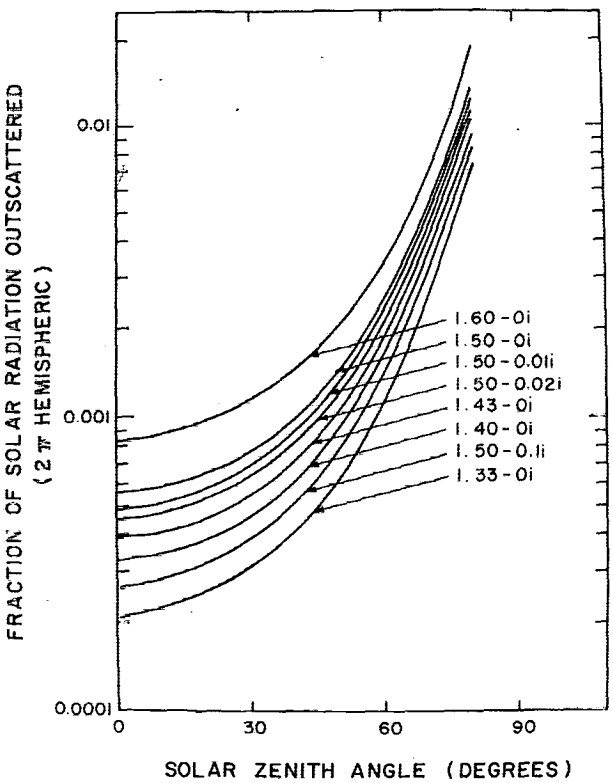

FIG. 14. Predicted values of the fraction of solar radiation outscattered at 0.53 μm wavelength by the stratospheric aerosol layer as a function of solar zenith angle for several refractive indexes and for a log-normal size distribution. The calculation assumes a globally uniform layer of stratospheric aerosol with 10^6 particles with diameter >0.3 μm per centimeter squared-column above the tropopause, the approximate condition for the 1971–73 period.

TABLE 5. Values of the stratospheric aerosol albedo at 0.53 μm wavelength for a log-normal size distribution and for a globally uniform layer of 10^6 particles with diameter $\geqslant 0.3$ μm per centimeter squared-column above the tropopause, the approximate condition during the 1971–73 period. The bracket marks the range of realistic values of the refractive index.

Aerosol refractive index	Fraction outscattered
$1.33-0i$	0.0014
$1.40-0i$	0.0019
$1.43-0i$	0.0022
$1.50-0i$	0.0028
$1.50-0.001i$	0.0028
$1.50-0.002i$	0.0028
$1.50-0.005i$	0.0028
$1.50-0.01i$	0.0027
$1.50-0.02i$	0.0025
$1.50-0.05i$	0.0021
$1.50-0.1i$	0.0017
$1.50-0.5i$	0.0012
$1.60-0i$	0.0038

4. Summary and conclusions

Several size distributions and composition models of the stratospheric aerosol have been fit to data from numerous global measurements by a balloon-borne photoelectric counter during 1971–73. Mie single scattering calculations for aerosol extinction, absorption, 180° backscattering, angular scattering, and 2π hemispheric backscattering have been presented for these size distributions and composition models. Resulting stratospheric optical depths are rather insensitive to particle refractive index and size distribution, within the range of size distributions that could possibly represent stratospheric aerosols. Absorption cross sections are nearly proportional to the aerosol refractive index absorptive part. Backscatter (180°) cross sections are relatively sensitive to particle refractive index but insensitive to size distribution. A particular comparison of predicted and measured lidar returns over Laramie in September 1972 show good agreement for several combinations of different size distributions and refractive indexes. A more accurate description of aerosol size distribution than that presented here would be difficult to obtain from multi-wavelength scattering measurements. The stratospheric aerosol albedo for these models is 0.002 to 0.003.

Acknowledgments. This research was supported by the Climatic Impact Assessment Program (CIAP) of the Department of Transportation through the Office of Naval Research and the Atmospheric Sciences Section and Office of Polar Programs of the National Science Foundation.

REFERENCES

Bhardwaja, P. S., J. Herbert and R. J. Charlson, 1974: Refractive index of atmospheric particulate matter: An *in situ* method for determination. *Appl. Opt.*, **13**, 731–734.

Bigg, E. K., 1975: Stratospheric particles. *J. Atmos. Sci.*, **32**, 910–917.

——, A. Ono and W. J. Thompson, 1970: Aerosols at altitudes between 20 and 37 km. *Tellus*, **22**, 550–563.

Braslau, N., and J. V. Dave, 1973a: Effect of aerosols on the transfer of solar energy through realistic model atmospheres. Part 1: Non-absorbing aerosols. *J. Appl. Meteor.*, **12**, 601-615.

——, and ——, 1973b: Effect of aerosols on the transfer of solar energy through realistic model atmospheres. Part II: Partly-absorbing aerosols. *J. Appl. Meteor.*, **12**, 616–619.

Dave, J. V., 1968: Subroutines for computing the parameters of the electromagnetic radiation scattered by a sphere. IBM Rept. 320–3237 [Available from IBM Scientific Center, Palo Alto, Calif.]

——, 1969a: Effect of coarseness of the integration increment on the calculation of the radiation scattered by polydispersed aerosols. *Appl. Opt.*, **8**, 1161–1167.

——, 1969b: Effect of varying integration increment on the computed polarization characteristics of the radiation scattered by polydispersed aerosols. *Appl. Opt.*, **8**, 2153–2154.

de Bary, E., and F. Rossler, 1966: Size distributions of atmospheric aerosols derived from scattered radiation measurements aloft. *J. Geophys. Res.*, **71**, 1011.

Deepak, A., and A. E. S. Green, 1970. Second and higher order scattering of light in a settling polydisperse aerosol. *Appl. Opt.*, **9**, 2362.

Elterman, L., R. B. Toolin and J. D. Essex, 1973: Stratospheric aerosol measurements with implications for global climate. *Appl. Opt.*, **12**, 330–337.

Grams, G. W., I. H. Blifford, Jr., B. G. Schuster and J. J. De Luisi, 1972: Complex index of refraction of airborne fly ash determined by laser radar and collection of particles at 13 km. *J. Atmos. Sci.*, **29**, 900–905.

——, ——, D. A. Gillette and P. B. Russell, 1974: Complex index of refraction of airborne soil particles. *J. Appl. Meteor.*, **13**, 459-471.

Green, A. E. S., G. D. Ward, T. Sawada, R. S. Sholtes, J. M. Schwartz, A. Deepak, D. Eisenhart, R. D. McPeters and B. D. Reller, 1972: Light scattering and the size-altitude distribution of atmospheric aerosols. *J. Colloid Interface Sci.*, **39**, 520–535.

Harrison, H., J. Herbert and A. P. Waggoner, 1972: Mie-theory computations of lidar and nephelometric scattering parameters for power law aerosols. *Appl. Opt.*, **11**, 2880–2885.

Hofmann, D. J., J. M. Rosen, T. J. Pepin and R. G. Pinnick, 1975: Stratospheric areosol measurements I: Time variations at northern midlatitudes. *J. Atmos. Sci.*, **32**, 1446–1456.

Latimer, P., 1972: Light scattering, data inversion, and information theory. *J. Colloid Interface Sci.*, **39**, 497-503.

Liou, Kuo-Nan, 1973: A numerical experiment on Chandrasekhar's discrete-ordinate method for radiative transfer: Applications to cloudy and hazy atmospheres. *J. Atmos. Sci.*, **30**, 1303–1326.

Northam, G. B., J. M. Rosen, S. H. Melfi, T. J. Pepin, M. P. McCormick, D. J. Hofmann and W. H. Fuller, Jr., 1974: Dustsonde and lidar measurements of stratospheric aerosols: A comparison. *Appl. Opt.*, **13**, 2416–2420.

Pilipowskyj, S., J. A. Weinman, B. R. Clemesha, G. S. Kent and R. W. Wright, 1968: Investigation of the stratospheric aerosol by infrared and lidar techniques. *J. Geophys. Res.*, **73**, 7553.

Pinnick, R. G., and D. J. Hofmann, 1973: Efficiency of light-scattering aerosol particle counters. *Appl. Opt.*, **12**, 2593–2597.

——, J. M. Rosen, and D. J. Hofmann, 1973: Measured light-scattering properties of individual aerosol particles compared to Mie scattering theory. *Appl. Opt.*, **12**, 37–41.

Plass, G. N., and F. W. Kattawar, 1972: Effect of aerosol variation on radiance in the Earth's atmosphere-ocean system. *Appl. Opt.*, **11**, 1598–1604.

Prishivalko, A. P., and Ye. K. Naumenko, 1973: Optical back-scattering and extinction coefficients of aqueous aerosol. *Izv. Atmos. Oceanic Phys.*, **9**, 660–663.

Rasool, S. I., and S. H. Schneider, 1971: Atmospheric carbon dioxide and aerosols: Effects of large increases on global climate. *Science*, **173**, 138–141.

Rosen, J. M., 1964: The vertical distribution of dust to 30 kilometers. *J. Geophys. Res.*, **64**, 4673–4696.

——, 1971: The boiling point of stratospheric aerosols. *J. Appl. Meteor.*, **10**, 1044–1046.

——, and D. J. Hofmann, 1974: Recent measurements of condensation nuclei from ground level to 25 km. Tech. Rept. CN-2, Dept. Phys. Astron., University of Wyoming.

——, —— and J. Laby, 1975: Stratospheric aerosol measurements II: The worldwide distribution. *J. Atmos. Sci.*, **32**, 1457–1462.

Sargent, S. L., and W. A. Beckman, 1973: A numerical model of thermal radiation in a dusty atmosphere. *J. Atmos. Sci.*, **30**, 88–94.

Shettle, E. P., and A. E. S. Green, 1974: Multiple scattering calculation of the middle ultraviolet reaching the ground. *Appl. Opt.*, **13**, 1567–1581.

Tashenov, R. T., E. L. Tem and I. A. Fedulin, 1973: Determinations of the atmospheric-aerosol spectrum from the optical characteristics of the clear daytime sky. *Izv. Atmos. Oceanic Phys.*, **9**, 314–317.

Ward, G., K. M. Cushing, R. D. McPeters and A. E. S. Green, 1973: Atmospheric aerosol index of refraction and size-altitude distribution from bistatic laser scattering and solar aureole measurements. *Appl. Opt.*, **12**, 2585–2592.

Yamamoto, G., and M. Tanaka, 1972: Increase of global albedo due to air pollution. *J. Atmos. Sci.*, **29**, 1405–1412.

Zuyev, V. Ye., L. S. Ivlev and K. Ya. Kondrat'yev, 1973: Recent results from studies of atmospheric aerosols. *Izv. Atmos. Oceanic Phys.*, **9**, 371–385.